

## **Brazilian Coastal Region Modeling with WRF/SMOKE/CMAQ and Atmospheric Parameter Measurement Validation with Radio Probing, Sodar and Lidar**

Ayres G. Loriato<sup>1</sup>, Nadir Salvador<sup>1</sup>, Ayran Ayres Barbosa Loriato<sup>2</sup>, Eric G. Sperandio Nascimento<sup>3</sup>, Davidson M. Moreira<sup>3</sup>, Neyval C. Reis. Jr.<sup>4</sup>, Anton Sokolov<sup>5</sup>, Eduardo Landulfo<sup>6</sup>, Taciana T. de A. Albuquerque<sup>7</sup>

<sup>1</sup>Universidade Federal do Espírito Santo – Industrial Technology Department, Brazil

<sup>2</sup>Instituto Tecnológico da Aeronáutica – Mechanical Engineering Department, Brazil

<sup>3</sup>SENAICIMATEC – Computational Modeling and Industrial Technology Department, Brazil

<sup>4</sup>Universidade Federal do Espírito Santo – Environmental Engineering Department, Brazil

<sup>5</sup>Université Lille Nord de France, Lille, France.

<sup>6</sup>IPEN – Instituto de Pesquisas Energéticas e Nucleares, IPEN, São Paulo, SP, Brazil

<sup>7</sup>Universidade Federal de Minas Gerais – Environmental and Sanitary Engineering Department, Brazil

---

### **ABSTRACT**

*This article aims to evaluate and compare data of vertical potential temperature profile, wind velocity and PM<sub>10</sub> concentration measured during an experimental campaign on July 2012 by means of radio probing, Sonic Detection And Ranging (SODAR) and Light Detection And Ranging (LIDAR) with those modeled by means of numerical simulation with Weather Research And Forecast Model (WRF), Sparse Matrix Operator Kernel Emissions (SMOKE) and Community Multi-Scale Air Quality (CMAQ). The study has been conducted at Região da Grande Vitória (RGV), a Brazilian coastal region. All data measurements have been done at Universidade Federal do Espírito Santo (UFES), in the city of Vitória, Espírito Santo, Brazil. For numerical simulation, RGV's emissions inventory has been used to model a 61x79km<sup>2</sup> grid with spatial resolution of 1 km<sup>2</sup> and temporal resolution of 1 hour. Sea breeze is a relevant weather phenomenon along coastal regions, and it has been perceived by both SODAR measurement and WRF modeling. During the experimental campaign, the most intense sea breeze occurred on July 28, 2012 and, therefore, a thorough analysis of atmospheric and pollution parameters has been done for that day. This analysis showed neutral atmosphere up to 200 meters of altitude and stability beyond that, which has been confirmed by WRF modeling. Regarding wind data, the comparison between SODAR measurement and WRF modeling showed similarities regarding wind direction, but wind speed was overestimated by WRF. Lastly, LIDAR measurement and CMAQ modeling showed close values for PM<sub>10</sub> pollutant concentration.*

---

Date of Submission: 14-01-2020

Date of Acceptance: 31-01-2020

---

### **I. INTRODUCTION**

Air pollutants transportation and dispersion patterns are heavily influenced by landform and soil characteristics, and this is even more noticeable in urban environments, where soil occupation is varied and complex. These patterns also suffer great variations on coastal regions, where ocean and continent air interact with each other. The way sea breeze flows into the land depends on various factors, such as its intensity, soil occupation complexity and the angle between the coast and the direction of dominant synoptic winds.

RGV is a coastal, industrial region, whose geographic position is peculiar with respect to sea breeze inflow, synoptic winds direction and soil occupation. These characteristics lead to distinct influences on air pollutants dispersion.

Due to its importance, air pollutants dispersion on urban centers near coast regions has attracted the attention of many researchers during recent years, such as Portelliet *al.* (1982), Jiménez *et al.* (2006), Bouchlaghemet *al.* (2007), Boyouket *al.* (2011), among others. However, the subject still raises many questions, such as performance evaluation on modeling of pollutants transportation and detailed simulations of it on the southern hemisphere.

Turbulent transportation, humidity, convection, lightning, dry and wet deposition are some of the meteorological processes that influence formation and transportation of primary and secondary pollutants. Numerical models are used to better understand the behavior of the atmosphere. These models of air quality analysis employ mathematical techniques to simulate physical and chemical processes occurring at the atmosphere (Castro e Apsley, 1997; Challa *et al.*, 2009).

---

Simon *et al.* (2012) reviewed the scientific literature between 2006 and March 2012, compiling and reviewing performance of several photochemical models using a wide array of statistical tools. During that period, CMAQ modeling was the researchers' preference, especially on studies regarding nitrates, ozone, PM<sub>2,5</sub> and sulfate.

Mathematical models allow forecasting future episodes and an in depth analysis of meteorological phenomena that induce air pollutants concentrations, but they must be collated with experimental measurements that characterize the aerosol, especially in urban areas (Chemelet *et al.*, 2010).

These models allow spatial and temporal representation of the distribution of pollutants concentrations on the atmosphere. Nevertheless, they might not be fully accurate due to the lack of ability, both of the model and of the data input, in faithfully reproducing soil and atmosphere characteristics. Another source of inaccuracy are atmospheric emissions inventories, which must always be updated because social and industrial dynamics change over time. Park *et al.* (2006) mention discrepancies on air quality modeling originate from various factors such as spatial variety of pollutants concentrations, emissions inventories, meteorological data, chemical mechanism parameters and numerical routines.

One of the critical aspects of photochemical modeling when studying air quality is the adequacy of the input emissions inventory which must include the main pollutants sources on the region of interest. These models suppose complete emissions data, including quantification, chemical characterization and temporal distribution. Therefore, model results are largely dependent on the quality and the detailing of atmospheric emissions in the studied area. All around the world, many researches are being carried out in order to obtain high resolution emissions inventories (Parra *et al.*, 2006; Jiménez *et al.*, 2006; Borgeet *et al.*, 2008; Cheng *et al.*, 2007; Imet *et al.*, 2010). In Brazil and in South America, the availability of emissions data is something to be considered, since there are few areas with complete and reliable emissions inventories. For RGV, there is the Instituto Estadual do Meio Ambiente e Recursos Hídricos' (IEMA) emissions inventory, which has been adapted by Loriao *et al.* (2018) to include emission factors of road resuspension according to Abu-Allaban *et al.* (2003), resulting on a grid with temporal resolution of 1 h and spatial resolution of 1x1km<sup>2</sup>. Albuquerque *et al.* (2018) have developed an emissions inventory for the city of São Paulo, Brazil, and its neighboring urban conglomerates, with temporal resolution of 1 h and spatial resolution of 3x3km<sup>2</sup>.

For this study, CMAQ photochemical modeling accuracy depends mainly on two factors. First, the meteorological modeling, in this case under sea breeze influence, made with WRF. Second, the IEMA's emissions inventory for RGV, which was adapted to SMOKE. There's a trend to compare WRF/SMOKE/CMAQ modeled values to those obtained experimentally from sources like LIDAR and SODAR (Vladutescu *et al.*, 2012; GANet *et al.*, 2011). Therefore, accuracy analysis involved comparison between modeled values and those obtained on experimental campaigns with SODAR, LIDAR and radio probing.

This work analyzed: i) potential temperatures measured by radio probing during the experimental campaign and compared them to those modeled with WRF; ii) wind speeds measured by SODAR during the experimental campaign and compared them to those modeled with WRF, particularly on day July 28, 2012; iii) wind directions measured by SODAR during the experimental campaign and compared them to those modeled with WRF, particularly on day July 28, 2012; iv) concentrations of PM<sub>10</sub> originated from anthropogenic and natural emissions measured by LIDAR on the evening of July 28, 2012 and compared them to those modeled with CMAQ.

## **II. MATERIAL AND METHODS**

This chapter describes the work developed during the research, including parameters used on the numerical models, devices used and data treatment.

### **2.1 Experimental Campaign on RGV**

The experimental campaign on RGV involved the usage of SODAR and LIDAR equipments collecting data between days July 24, 2012 and July 31, 2012.

#### **2.1.1 SODAR**

The SODAR used, a Scintec MFAS: *Flat Array Sodar*, belongs to Universidade Estadual Paulista (UNESP) and its operation on RGV was supervised by Professor Doctor Gerhard Held from Instituto de Pesquisas Meteorológicas (IPMET), which is linked to UNESP. It emits 10 frequencies (1650 – 2750 Hz) and was programmed for a vertical resolution of 10 m, from 30 m of altitude up to 800 m, with moving average of 30 minutes. Figure 2.1 shows the SODAR installed on the UFES campus during the experimental campaign on RGV. There are other experimental researches of similar atmospheric phenomena (Mestayer *et al.*, 2005; Bastinet *et al.*, 2006; Muppa *et al.*, 2012).



**Figure 2.1: SODAR operating during the experimental campaign on RGV.**

### 2.1.2 LIDAR

The LIDAR used belongs to the Centro de Laser Aplicado (CLA) of Instituto de Pesquisas Energéticas e Nucleares (IPEN) linked to Universidade de São Paulo (USP). Its operation was coordinated by Professor Doctor Eduardo Landulfo. This campaign is the result of the relationship and partnership between air pollution researchers from UFES and USP, which made possible the aforementioned usage of equipments and professional support. The model used was an Nd:YAG Laser – Quantel CFR 200, with wavelength of 532 nm, repetition rate of 20 Hz, beam divergence less than 0.5 mrad, Cassegrain telescope with 20 cm diameter, field of vision (FOV) of 1 mrad, overlap of 180 m, two photomultiplier tubes (PMTs), detection channels of 532 and 607 nm, interference filters of 1 nm and vertical resolution of 7.5 m. Figure 2.2 shows the LIDAR operating on the UFES campus. There are many experimental researches of atmospheric phenomena and aerosol presence in Brazil and in other countries (Melfiet *et al.*, 1985; Menut *et al.*, 1999; Murayama *et al.*, 1999; Landulfo *et al.*, 2003; Mestayer *et al.*, 2005; Landulfo *et al.*, 2007; Talbot *et al.*, 2007 a, b; Landulfo *et al.*, 2009; Gao *et al.*, 2011; Vladutescu *et al.*, 2012; Salvador *et al.*, 2016 a, b). LIDAR devices have also been used to study volcanic aerosol emissions such as in Ansmann *et al.* (1996), who focused on the Pinatubo volcano eruption in Philippines, and in Porter *et al.* (2002), who focused on the Kilauea volcano eruption in Hawaii.

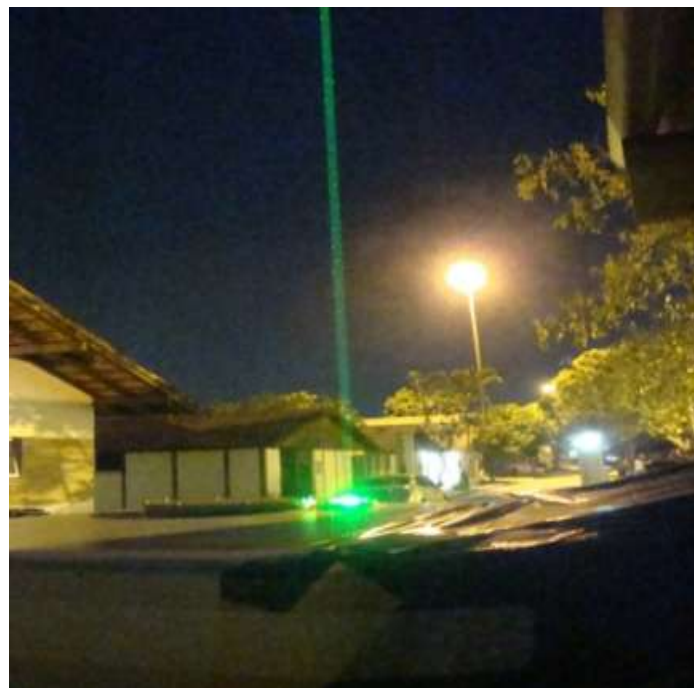


**Figure 2.2: LIDAR operating during the experimental campaign on RGV.**

## 2.2 Numerical Simulations and Data

Numerical modeling employed WRF 3.5.1, *Meteorology-Chemistry Interface Processor* (MCIP), SMOKE and CMAQ. CMAQ requires the following input in order to calculate concentrations results: meteorological data, which are provided by WRF and adapted by MCIP; emissions inventory data processed by SMOKE; boundary and initial conditions; photolysis rates.

### 2.2.1 WRF Meteorological Model for RGV

Aiming for better results for the meteorological modeling, different parameterizations combinations were tested (Salvador, 2016). Inadequate parameterization is one of the observed sources of errors on photochemical modeling.

Final parameters adopted included *NOAH Land Surface Model* as the soil layer (*sf\_surface\_physics*), *MM5 similarity Monin-Obukov* as the surface layer (*sf\_sfclay\_physics*), *Yonsei University Scheme (YUS)* as the atmospheric boundary layer (*bl\_pbl\_physics*) and *NOAHsf\_surface* as the number of soil layers (*num\_soil\_layers*).

WRF grid nesting for RGV encompassed four domains, as shown on Figure 2.3. The first domain (d\_01), with 35x35 cells of 27x27km<sup>2</sup> each, covers the states of Espírito Santo, Rio de Janeiro and parts of Minas Gerais and Bahia; the second domain (d\_02), with 55x55 cells of 9x9km<sup>2</sup> each, covers Espírito Santo and parts of Rio de Janeiro, Minas Gerais and Bahia; the third domain (d\_03), with 82x82 cells of 3x3km<sup>2</sup> each, covers Espírito Santo's central and southern regions; lastly, the fourth domain (d\_04), with 120x120 cells of 1x1km<sup>2</sup> each, covers RGV and part of the Atlantic Ocean. They are all centered at latitude 20.251147° S and longitude 40.285506° W.

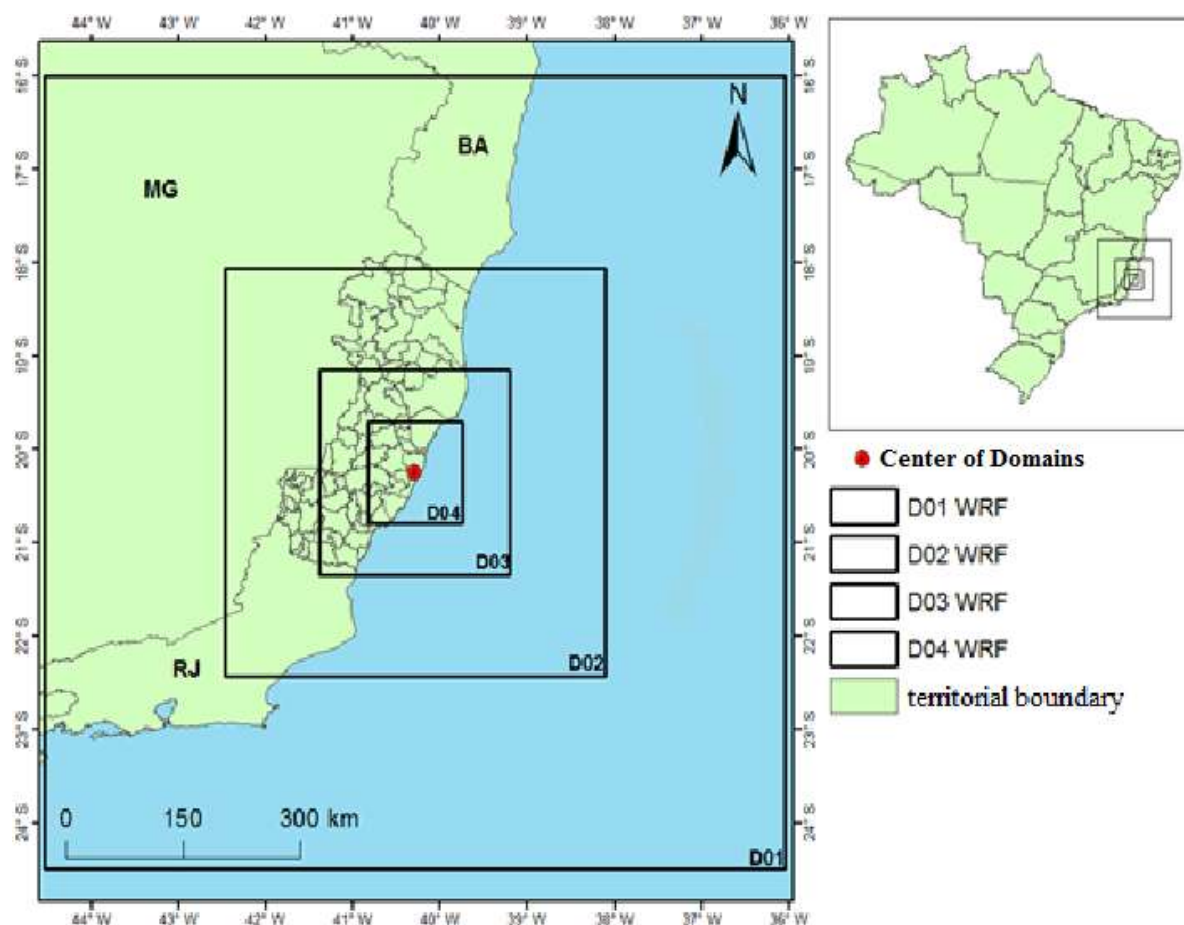


Figure 2.3: WRF domains on RGV.

The number of vertical layers used was 20, of which 9 were below 515 m of altitude. The layer of interest for CMAQ is d\_04, which was processed by MCIP, leaving it with 61x79 cells of 1x1km<sup>2</sup> each. Main temporal and spatial parameterizations used are found on Table 2.1 below.

**Table 2.1: WRF's temporal and spatial parameters used for RGV.**

Temporal parameters				
Starting date	07/15/2012, 00:00 UTC			
Final date	07/31/2012, 24:00 UTC			
Duration	408 hours			
Spatial parameters				
Grid resolutions	27 km	9 km	3 km	1km
Number of columns	36	55	82	121
Number of rows	36	55	82	121
Number of vertical layers	21			
Center of reference	-20.251147°; -40.285506°			

**2.2.2 MCIP (Meteorology-Chemistry Interface Processor).**

One of the MCIP's functions is to eliminate some border cells from WRF innermost domain in order to avoid boundary problems when passing from domain d\_03 to d\_04. BTRIM, the MCIP variable responsible for this operation, was set to -1, eliminating 59 rows and 41 columns from d\_04, originally containing 120x120 cells, resulting in a CMAQ domain with 61x79 cells of 1x1km<sup>2</sup> each, as shown on Figure 2.4. CMAQ domain's center of reference is the same as WRF domains' shown on Table 2.2, and it is located at Vitória's airport station.

**2.2.3 SMOKE (Sparse Matrix Operator Kernel Emissions)**

Some adaptations were needed on the RGV's emissions inventory for use with SMOKE, as shown on table 2.2, based in Abu-Allaban *et al.*, 2003 e Loriato *et al.*, 2018. The most remarkable one was a new estimate on vehicle emissions due to resuspension, since the values provided by IEMA's inventory were considered relatively high in comparison with other Brazilian and foreign cities. SPECIATEv4.2 database, provided by the United States Environmental Protection Agency (USEPA, 2009), was used for chemical speciation. Biogenic emissions were estimated by the MEGAN model.

**Table 2.2: RGV's emissions by type of source, in percentage, adjusted with road traffic resuspension.**

Type of source	PM <sub>10</sub>	PM <sub>2,5</sub>	SO <sub>2</sub>	NO <sub>x</sub>	CO	NMVOC
% diffuse	18,56	17,52	22,59	17,98	0,84	39,43
% punctual	13,86	27,95	76,04	48,64	49,54	6,92
% road	67,58	54,53	1,37	33,38	49,61	53,65

Source: Adapted from IEMA\_ES (2011).

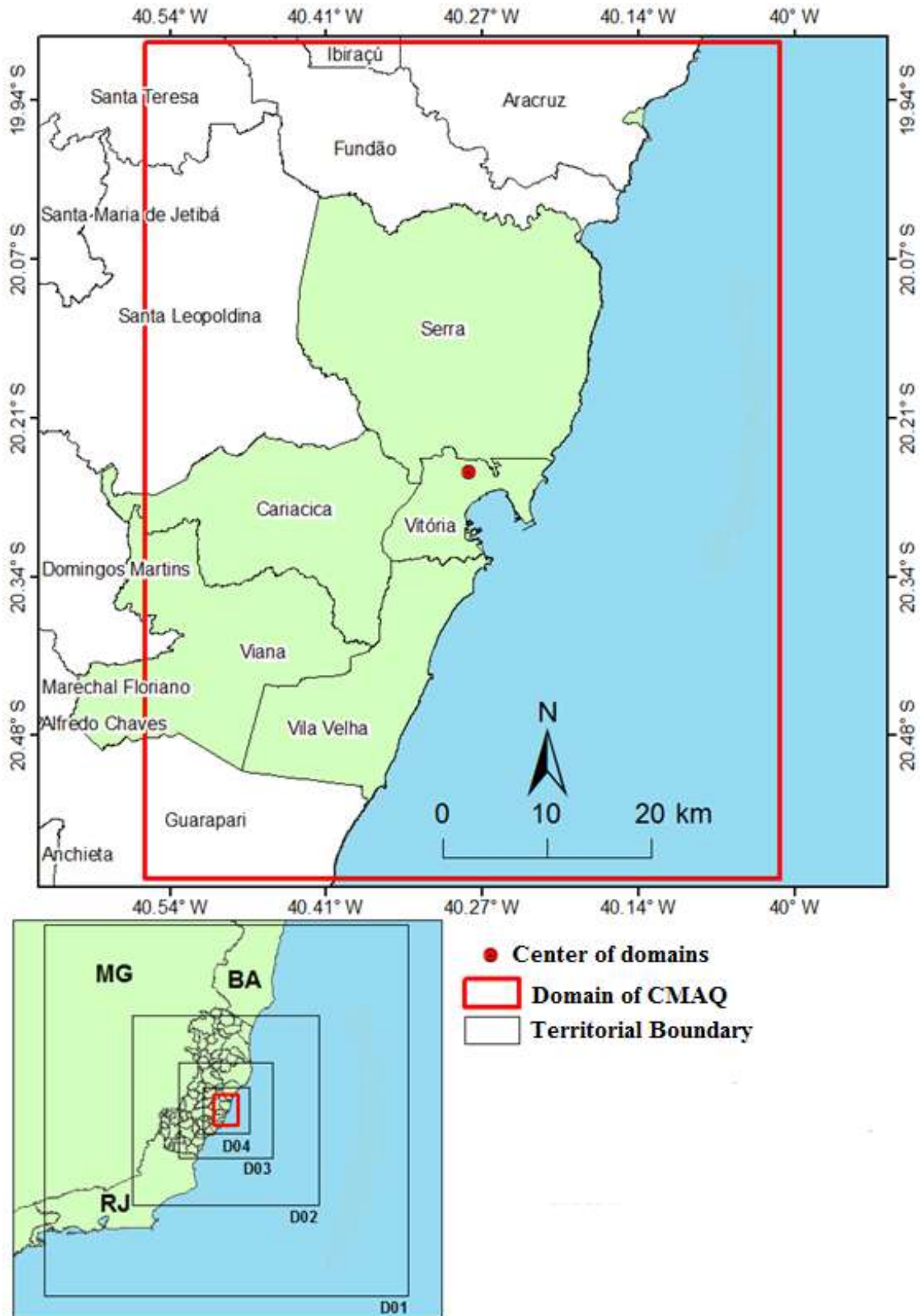


Figure 2.4: CMAQ domain of interest for RGV, as defined by MCIP.

### 2.2.4 Initial Conditions (ICON) and Boundary Conditions (BCON)

CMAQ system has a predefined set of profiles that can be used to generate initial and boundary conditions. These profiles provide species concentrations as a function of the altitude and are spatially independent for the initial conditions preprocessor (ICON) and minimally independent for the boundary conditions preprocessor (BCON). Both profiles are time independent. Since data don't have a high resolution, these profiles are used when there is no information available about the initial and boundary conditions (Gipson, G.L., 2009).

For the RGV simulation, initial and boundary conditions used were the default provided by the model mentioned above. These conditions were used during the first processing of ICON and BCON. Subsequent processing used species concentration obtained from the previous processing as initial and boundary conditions.

### 2.2.5 Photolysis rates (JPROC)

Data of extraterrestrial radiation, absorption, scattering and surface albedo are directly provided by radioactive model *Clear-sky Photolysis Rate Calculator* (JPROC). These rates vary according to meteorological conditions. JPROC calculates the actinic flux under clear sky and then *CMAQ Chemical Transport Model* (CCTM) attenuates it when nebulosity is present. JPROC calculates each photolysis reaction rate in various latitudes, altitudes and zenith angles. Inside CCTM, the PHOT sub-routine interpolates JPROC generated data to individual grid cells and adjusts itself for cloud presence.

### 2.2.6 CMAQ Chemical Transport Model (CCTM)

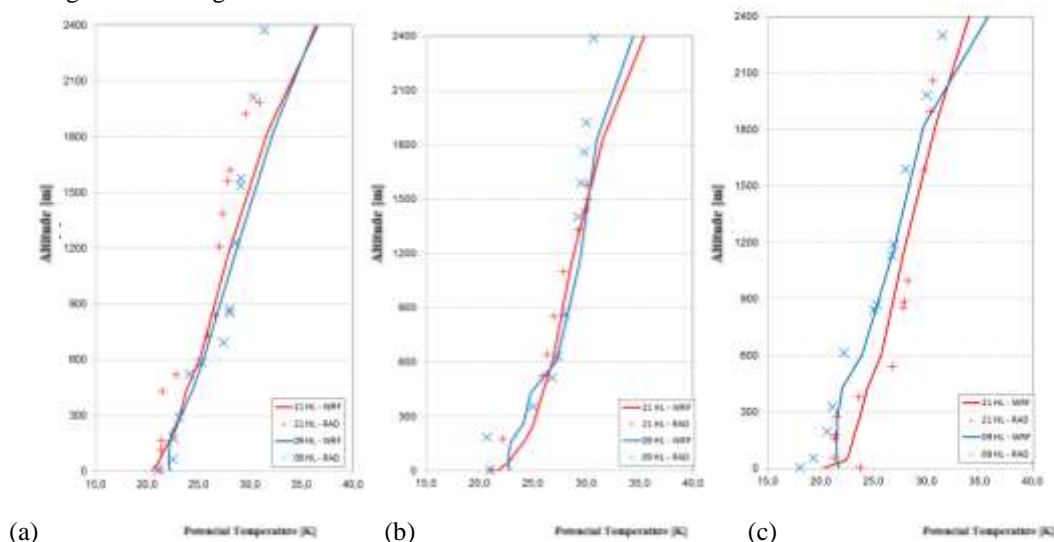
CCTM conjugates data from MCIP, ICON, BCON and JPROC preprocessors, as well as emissions input on CMAQ format (such as the output from SMOKE), to continuously simulate atmosphere chemical conditions. Relevant species concentrations can be captured at a predetermined time frequency, often hourly. CCTM output files are all binaries and contain air pollution information, such as gas phase, aerosols, dry and wet deposition, visibility and average concentrations, resolved temporally on grids. CCTM spatial and temporal coverage is dictated by meteorological input information.

## III. RESULTS FOR RGV

### 3.1 Potential temperature: comparison between Probing Radio (RAD) and WRF

Vertical profiles of potential temperature simulated by WRF and measured by Vitória Airport's radio probing station during the experimental campaign are shown and compared on Figures 3.1 (a) to (j). Measurements were taken every day at 09:00 and at 21:00. The simulation was able to reasonably represent temperature values, however at low altitudes there is a greater discrepancy between modeled and measured values. In general, at 09:00 WRF tends to underestimate measured values and at 21:00 WRF tends to overestimate them.

At 21:00, the WRF model presented stable atmosphere at ground level on all days, except July 30, 2012, when it showed neutral atmosphere, i.e, red line perpendicular to the potential temperature axis at ground level. This makes sense, since it is usual to have atmospheric stability at night. Due to the scantiness of the radio probing station measurements, a more detailed analysis was not possible. Still, the station confirmed the neutral atmosphere on July 30, 2012, but it indicated unstable atmosphere on days July 24, 2012 and July 29, 2012, contradicting the modeling.



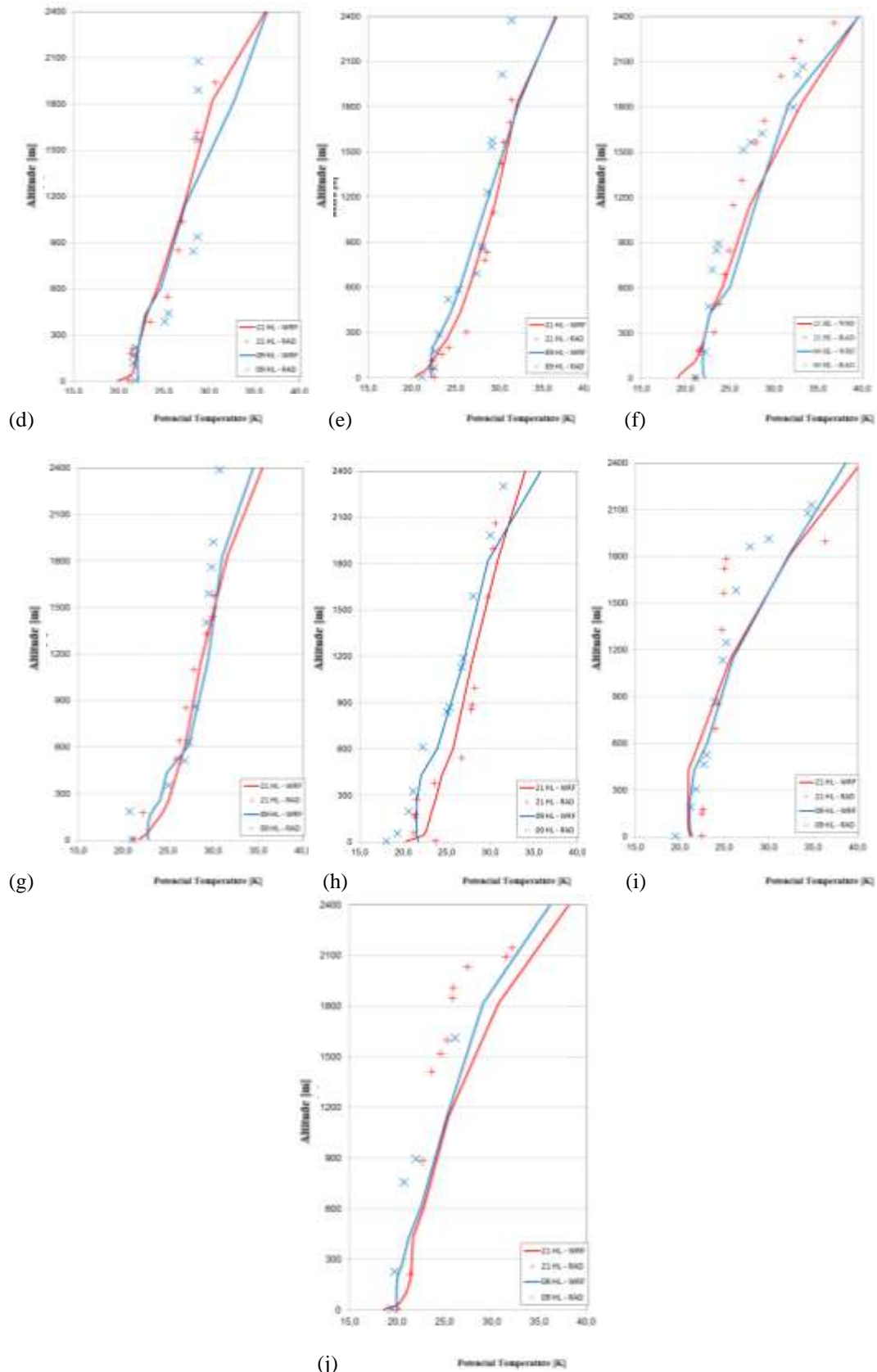
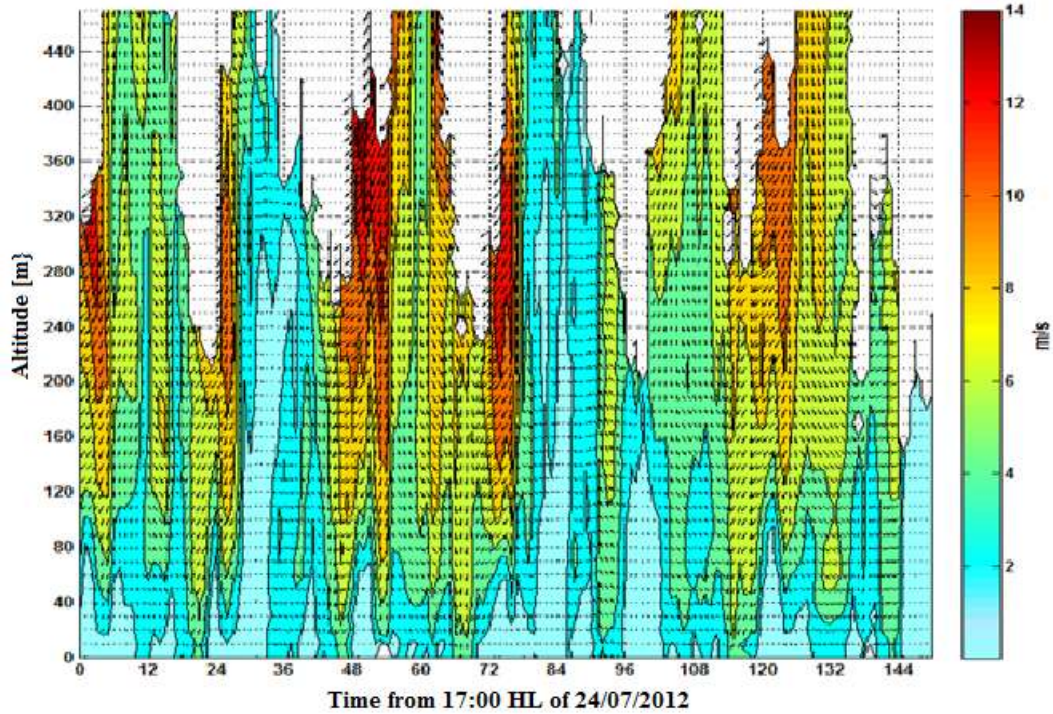


Figure 3.1 (a-j): Potential temperature profiles on RGV modeled by WRF-line blue at 9:00 HL (12:00 GMT) and WRF-line red at 21:00 HL (24:00 GMT) and measured by the airport radio probing station- x blue at 9:00 HL (12:00 GMT) and airport radio probing station- + red at 21:00 HL (24:00 GMT) on days: (a) 2012/07/22; (b) 2012/07/23; (c) 2012/07/24; (d) 2012/07/25; (e) 2012/07/26; (f) 2012/07/27; (g) 2012/07/28; (h) 2012/07/29; (i) 2012/07/30; (j) 2012/07/31.

### 3.2 Wind Velocity Field: comparison between SODAR and WRF

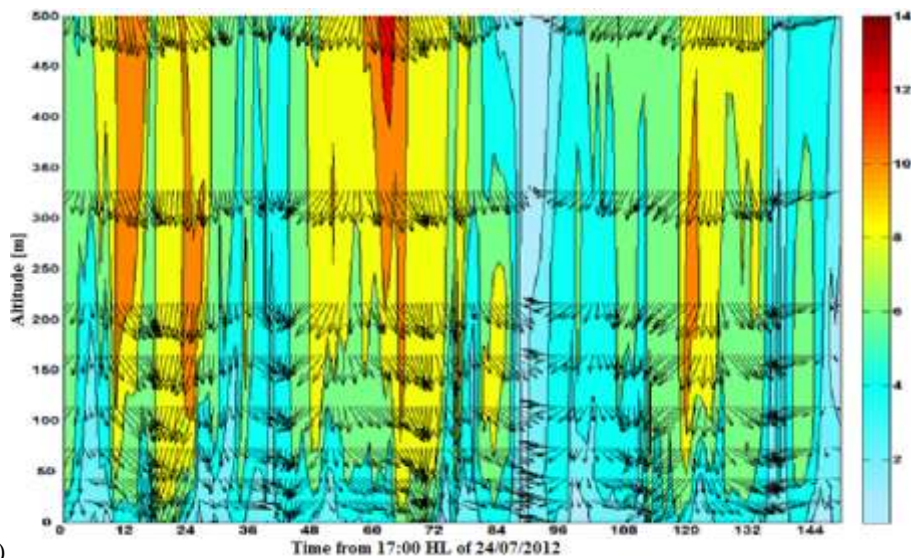
A detailed observation of Figure 3.2a indicates that on abscissa 91 (July 28, 2012 12:00) there is an abrupt change in the wind direction and a lowering of its speed, and this last fact is also noticeable on Figure 3.2b. These behaviors can be explained by the presence of sea breeze inflow. Therefore, a more detailed analysis was made on day July 28, 2012, as shown on Figures 3.3a and 3.3b.

Two important facts are observed by comparing Figures 3.3a and 3.3b. The first one is that WRF simulation tends to overestimate wind speed module. The second one is the abrupt change in the wind direction around 12:00, corroborating the sea breeze inflow at that moment. Moreover, SODAR data show a more gradual change in the wind direction than WRF prediction, which indicates a sudden change in the wind direction in a time interval of only 1 hour.



(a)

Figure 3.2: (a) Wind velocity field on RGV measured by SODAR between 2012/07/24 17:00 and 2012/07/30 16:00.



(b)

Figure 3.2: (b) Wind velocity field on RGV calculated by the WRF model between the same dates and times.

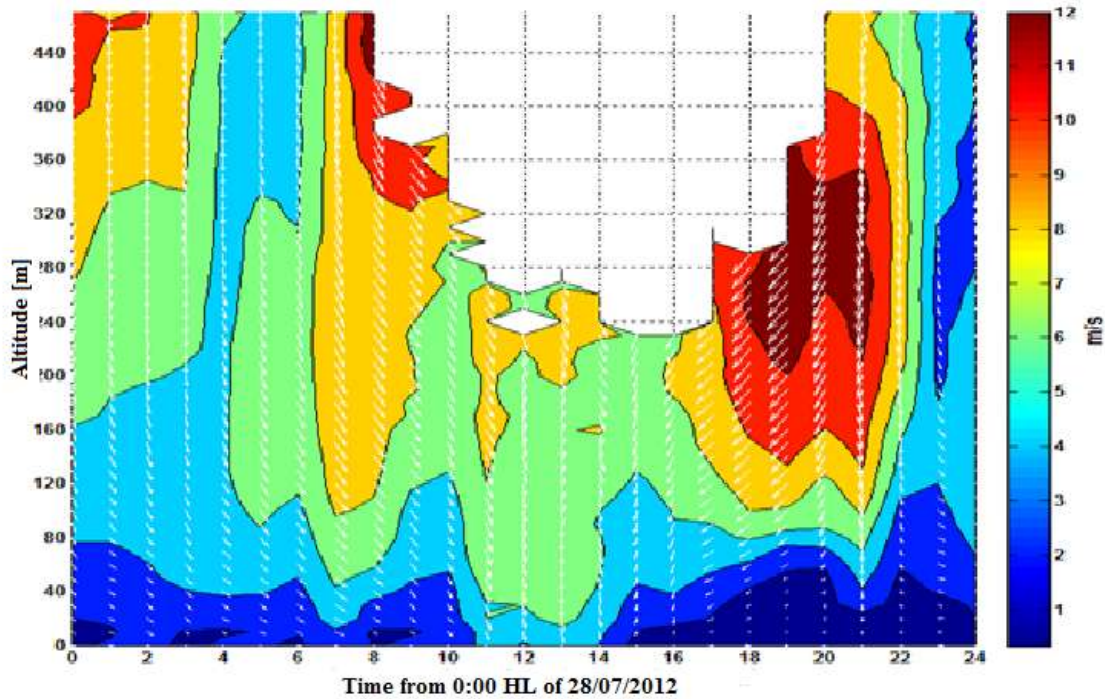


Figure 3.3(a): Wind velocity field on RGV measured by SODAR on 2012/07/28.

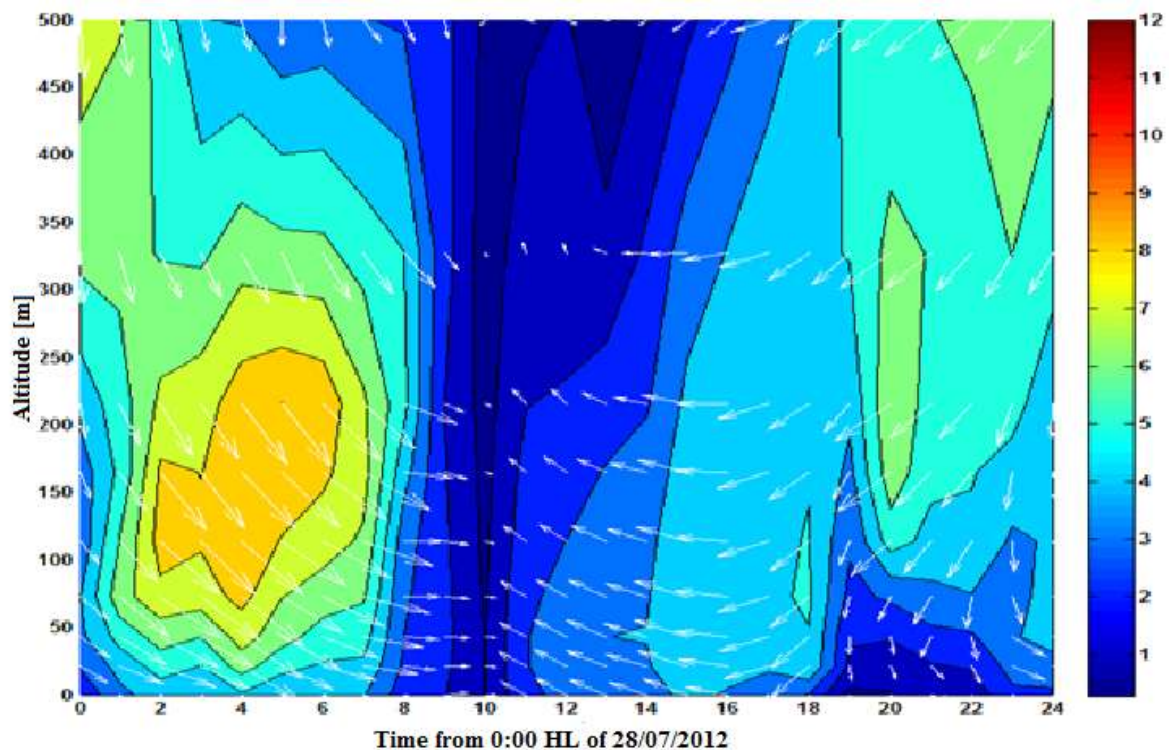


Figure 3.3(b): Wind velocity field on RGV calculated by the WRF model on 2012/07/28.

### 3.3 Wind velocity at the first altitude measured by SODAR (30 m): comparison between SODAR and WRF

Comparing SODAR and WRF wind velocity at the lowest altitude measured by SODAR is important because the majority of the population on RGV live in these low altitudes and, therefore, the knowledge of air pollutant transportation is more useful there. During the experimental campaign at UFES, the first measurement taken by SODAR was at an altitude of 30 m.

For wind speed module, Figure 3.4 shows that WRF simulated values are sensibly higher than the measured ones. However, the simulation does follow the variation trends experimentally measured.

Figure 3.5 compares measured and modeled values of wind direction. It is noticed that both wind direction module and variation are well represented by the simulation. Statistical analysis results are shown on Table 3.1.

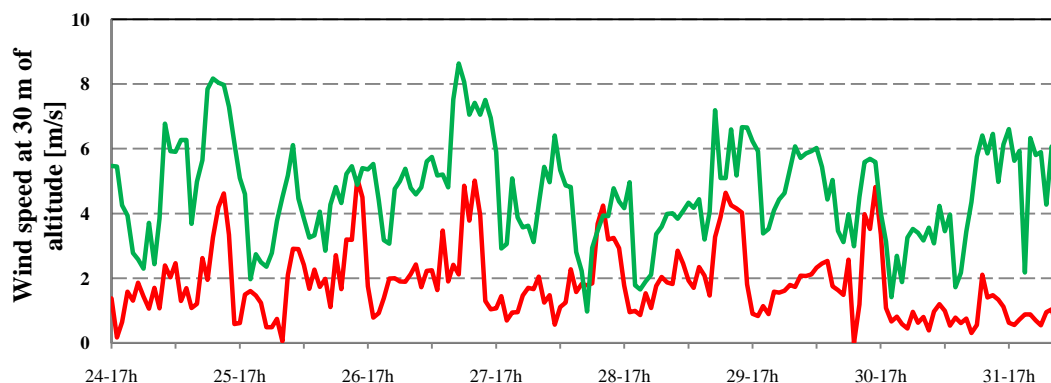


Figure 3.4: Wind speed module on RGV at 30 m of altitude as simulated by WRF (green) and as measured by SODAR (red).

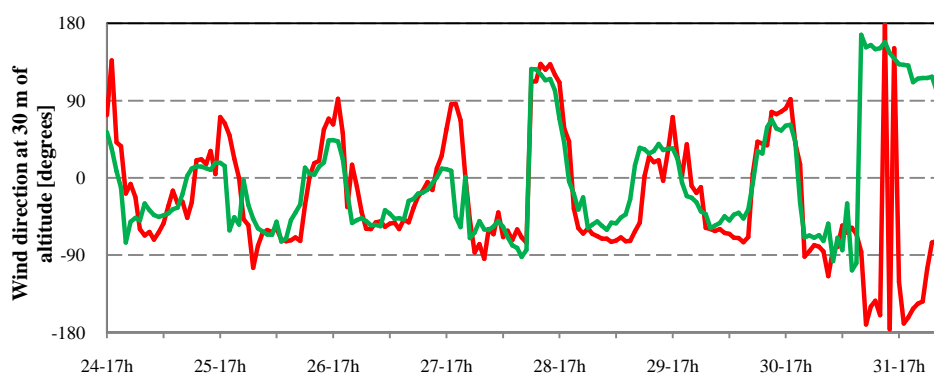


Figure 3.5: Wind direction on RGV at 30 m of altitude as simulated by WRF (green) and as measured by SODAR (red).

Table 3.1: Statistical parameters between WRF simulation and SODAR measurements of wind velocity on RGV at 30 m of altitude

SODAR/WRF	Wind Speed (m/s)	Wind Direction (°)
Number of observations	175	175
Measured average	1,9	212,5
Simulated average	4,6	214,0
Measured standard deviation	1,1	119,3
Simulated standard deviation	1,6	128,2
RATIO	4,0	2,7
BIAS	2,8	1,6
NMB	1,5	0,0
NMSE	1,3	0,02
r	0,4	0,7
r <sup>2</sup>	0,2	0,5

### 3.4 Aerosol layer: comparison between CMAQ and LIDAR

It was only possible to put the LIDAR device at UFES in operation at July 28, 2012 14:25, so a better visualization of the sea breeze inflow was prevented. However, as shown on Figure 3.6a, a significant high in the vertical aerosol layer is noticeable. It decreases until about 16:00, and increases again after that time. Figure 3.6b represents the  $PM_{10}$  concentration simulated by CMAQ, and the purple line indicates the atmospheric boundary layer (ABL) generated by WRF, starting at 14:00, for comparison with LIDAR measurements.

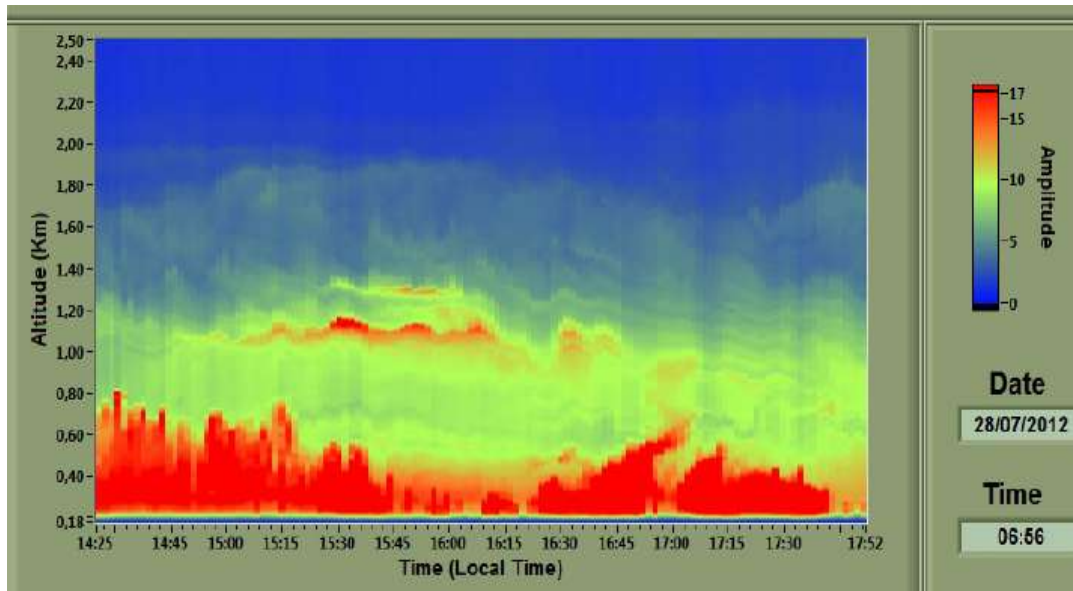


Figure 3.6a: Vertical aerosol layer detected by LIDAR between 2012/07/28 14:25 and 17:52, with correction for background radiation and altitude due to the magnetic field decrease with the squared value of altitude.

Source: Moreira (2013).

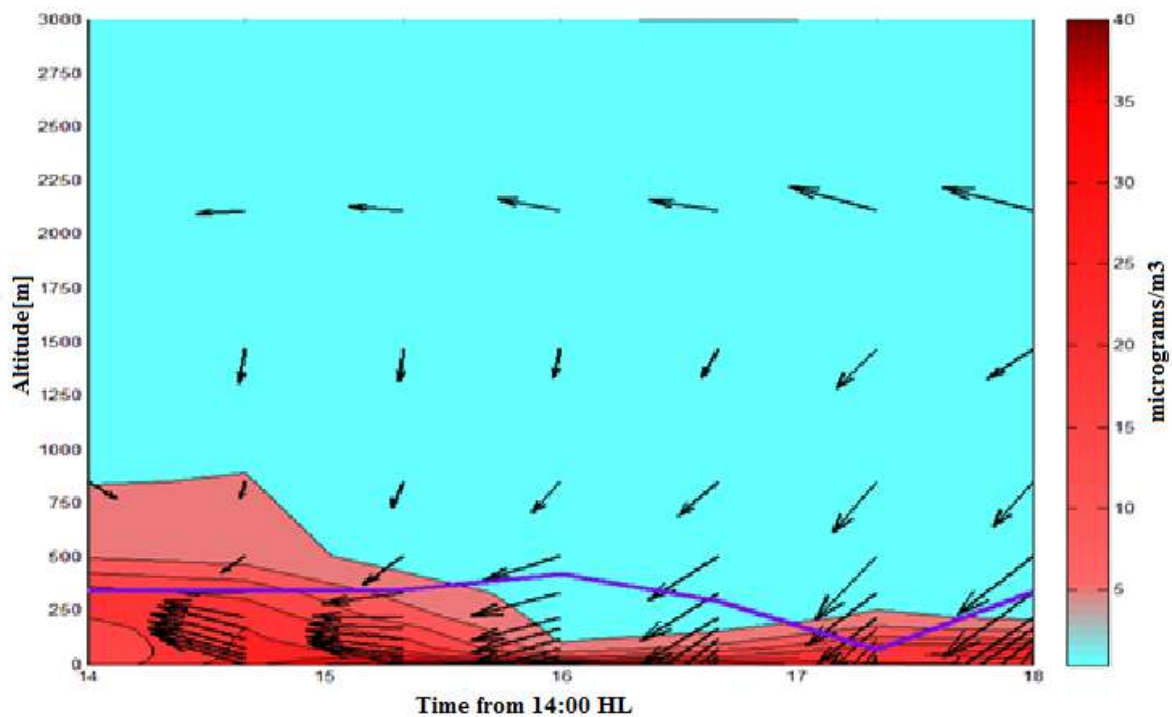


Figure 3.6b: Vertical aerosol layer simulated, speed vectors and atmospheric boundary layer (line purple) by CMAQ between 2012/07/28 14:00 and 18:00.

Simulated  $PM_{10}$  presence is intense between 14:00 and 15:00, particularly at low altitudes.

Figure 3.7 shows the overlap of LIDAR measurement and CMAQ simulation. The results are quite close, especially considering the inherent limitations of computation modeling.

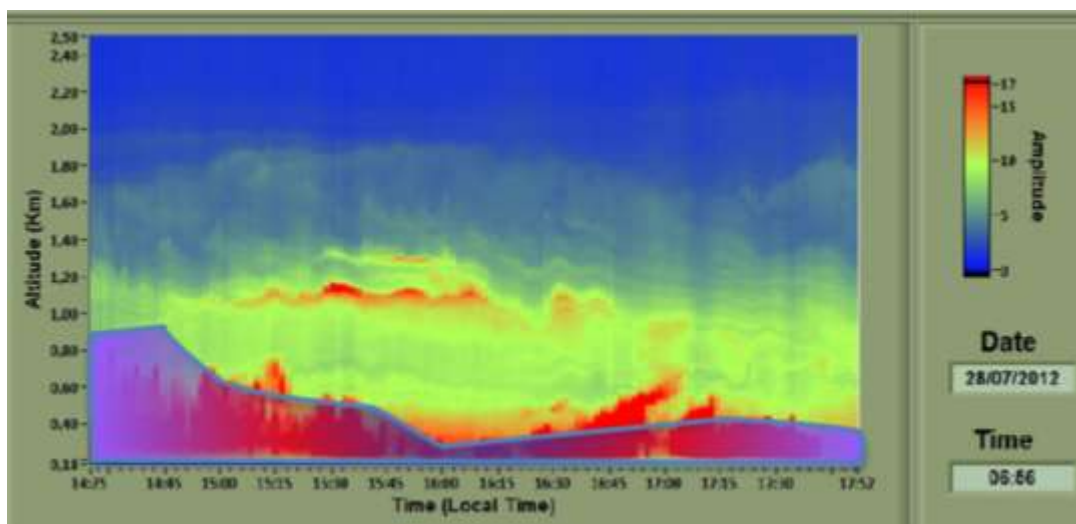


Figure 3.7: LIDAR measurement and CMAQ simulation overlap.

#### IV. CONCLUSIONS

Experimental measurements of potential temperature taken by the radio probing station showed divergences with the WRF modeling, and in some days the interpretation about the type of atmosphere (neutral, stable or unstable) did not coincide. This might be due to the scantiness of the radio probing measurements: only twice a day. In this analysis, both radio probing and WRF simulation indicated neutral atmosphere up to 200 m of altitude and stability beyond that.

The wind velocity analysis allowed for the identification of the sea breeze inflow on July 28, 2012 at around 12:00, and this was noticeable both on the SODAR experiment and the WRF simulation. The identification of this phenomenon is extremely important on industrialized coastal regions, because it may be the main factor on the transportation of air pollutants to more densely populated areas. A thorough analysis of wind speed and direction was performed on this day, with particular interest at the lowest measured altitude of 30 m, where the wind more heavily impacts people's lives. Regarding wind speed module at this altitude, the WRF model showed sensibly higher values than the measured ones, but both simulation and measurements follow the same variation trends. The modeling of wind direction achieved good results in comparison with measured values, resulting in small percent error.

Aerosol simulation with CMAQ between shows good adherence to LIDAR measurements during the same period. This result corroborates Vladutescu *et al.*, (2012) observation that CMAQ aerosol modeling achieves better performance on stable atmospheres.

This study shows the importance of comparing experimental measurements of atmospheric phenomena and pollution with numerical modeling. Both are important and complement each other, allowing for improved data so that regulatory agencies can develop public policies that ensure a better quality of life for the population and future generations. It is important to notice that studies like this are rare on the southern hemisphere, where the availability of reliable information, especially inventory emissions, is scarce.

#### REFERENCES

- [1]. Abu-Allaban, M., Gillies, J.A., Gertler, A.W., Clayton, R., Proffitt, D. Tailpipe, resuspended road dust, and brake-wear emission factors from on-road vehicles. *Atmospheric Environment*, v. 37, p. 5283-5293, 2003.
- [2]. Albuquerque, T.T.A., Andrade, M. F., Miranda, Ynoue, R. Y., Moreira, D. M., Andreão, W. L., Santos, F. S., Nascimento, E. G.S. WRF-SMOKE-CMAQ modeling system for air quality evaluation in São Paulo megacity with a 2008 experimental campaign data. *Environmental Science and Pollution Research* <https://doi.org/10.1007/s11356-018-3583-9>, 2018.
- [3]. Ansmann, A., Mattis, I., Wandinger, I., Wagner, F. Evolution of the Pinatubo Aerosol: Raman Lidar Observations of Particle Optical Depth, Effective Radius, Mass, and Surface Area over Central Europe at 53.48N. *Journal of the Atmospheric Sciences*, v. 54, p. 2630-2641, 1996.
- [4]. Bastin, S., Drobinsk, P. Sea-breeze-induced mass transport over complex terrain in south-eastern France: A case-study. *Q. J. R. Meteorol. Soc.*, 132, pp. 405–423 doi: 10.1256/qj.04.111, 2006.
- [6]. Borge, R., Lumbreras, J., Rodríguez, E., 2008. Development of a high-resolution emission inventory for Spain using the SMOKE modelling system: A case study for the years 2000 and 2010. *Environmental Modelling & Software*, v. 23, p. 1026-1044, 2008.
- [7]. Bouchlaghem, K. Mansour, F.B. Elouragini, S. Impact of a sea breeze event on air pollution at the Eastern Tunisian Coast. *Atmospheric Research*, 86, 162 – 172. 2007.
- [8]. Boyouk, N., León, J.F. Delbarre, H. Augustin, P. Fourmentin, M. Impact of sea-breeze on vertical structure of aerosol optical properties in Dunkerque, France. *Atmospheric Research*, 101, 902 – 910. 2011.
- [9]. Castro, I. P.; Apsley D. D. Flow and Dispersion Over Topography: A Comparison Between Numerical and Laboratory Data For Two-Dimensional Flows. *Atmospheric Environment*, V.31, p. 839-850, 1997.

- [10]. Challa, V.S.;Indracanti, J.; Rabarison, M.K.; Patrick, C.; Baham, J.M.; Young, J.; Hughes, R.; Hardy, M.G.; Swanier, S. J.; Yerramilli, A. A simulation study of mesoscale coastal circulations in Mississippi Gulf coast. *Atmospheric Research*, v. 91, i. 1, p. 9 – 25, 2009.
- [11]. Chemel, C.; Sokhi, R.S.; Yu, Y.; Hayman, G.D.; Vincent, K.J.; Dore, A.J.; Tang, Y.S.; Prain, H.D.; Fisher, B.E.A. Evaluation of a CMAQ simulation at high resolution over the UK for the calendar year 2003. *Atmospheric Environment*, v. 44, p. 2927-2939, 2010.
- [12]. Cheng S., Chen D., Li, J., Wang, H., Xiuruiguo, X. The assessment of emission-source contributions to air quality by using a coupled MM5-ARPS-CMAQ modeling system: A case study in the Beijing metropolitan region, China. *Environmental Modelling & Software*, v. 22, p. 1601-1616, 2007.
- [13]. Gan, C.M., Wu, Y., Gross, B., Moshary, F., Madhavan, B., L. Application of active optical sensors to probe the vertical structure of the urban boundary layer and assess anomalies in air quality model PM2.5 forecasts. *Atmospheric Environment*, 45 (2011) 6613e6621.
- [14]. Gao, F., Bergant, K., Filipic, A., Forte, B., Hua, D. X., Song, X. Q., Stanic, S., Veberic, D., Zavrtnik, M. Observations of the atmospheric boundary layer across the land–sea transition zone using a scanning Mie lidar. *Journal of Quantitative Spectroscopy & Radiative Transfer* 112 (2011) 182–188.
- [15]. Gipson, G.L., 2009. The Initial Concentration and Boundary Condition Processors\_Ch13 in *Science Algorithms of the EPA Models-3 Community Multiscale Air Quality (CMAQ) Modeling System*, EPA-600/R-99/030.
- [16]. Im, U., Markakis, K., Unal, A., Kindap, T., Poupkou, A., Incecik, S., Yenigun, O., Melas, D., Theodosi, C., Mihalopoulos, N. Study of a winter PM episode in Istanbul using the high resolution WRF/CMAQ modeling system. *Atmospheric Environment*, v.44, p. 3085-3094, 2010.
- [17]. Jiménez, P., Jorba, O., Parra, R., Baldasano, J.M. Evaluation of MM5-EMICAT2000-CMAQ performance and sensitivity in complex terrain: High-resolution application to the northeastern Iberian Peninsula. *Atmospheric Environment*, 40 (2006) 5056–5072.
- [18]. Landulfo, E., Papayannis, A., Artaxo, P., Castanho, A.D.A., Freitas, A.Z., Souza, R.F., Vieira Junior, N.D., Jorge, M.P.M.P., Sánchez-Ccoyllo, O.R., Moreira, D.S., 2003. Synergetic measurements of aerosols over São Paulo, Brazil using LIDAR, sunphotometer and satellite data during the dry season. *Atmos. Chem. Phys.* 3, 1523–1539, 2003.
- [19]. Landulfo, E., Matos, C.A., Torres, A.S., Sawamura, P., Ueharas, T., 2007. Air quality assessment using a multi-instrument approach and air quality indexing in an urban area. *Atmospheric Research*. 85 (2007) 98–111.
- [20]. Landulfo, E., Freitas, A.Z., Longo, K.M., Uehara, S.T., Sawamura, P., 2009. A comparison study of regional atmospheric simulations with anelastic backscattering Lidar and sunphotometry in an urban area. *Atmos. Chem. Phys.* 9, 6767–6774, 2009.
- [21]. Loriato, A.G., Salvador, N., Loriato, A.A.B., Sokolov, A., Nascimento, A.P., Ynoue, R.Y., Moreira, D.M., Reis, N. C., Albuquerque, T.T.A. Inventário de Emissões com Alta Resolução para a Região da Grande Vitória Utilizando o Sistema de Modelagem Integrada WRF-SMOKE-CMAQ. *Revista Brasileira de Meteorologia*, v. 33, n. 3, 2018
- [22]. Melfi, S.H., Spinhirne, J.D., Chou, S.H., Palm, S.P. Lidar observations of the vertically organized convection in the planetary boundary layer over ocean. *J. Clim. Appl. Meteorol.*, 24, 806–821, 1985.
- [23]. Menut, L., Flamant, C., Pelon, J., Flamant, P.H. Urban boundary layer height determination from Lidar measurements over the Paris area. *Appl. Opt.*, 38, 945–954, 1999.
- [24]. Mestayer, P.G., Durand, P., Augustin, P., Bastin, S., et al. The Urban Boundary-Layer Field Campaign In Marseille (UBL/CLU-Escompte): Set-Up And First Results. *Boundary-Layer Meteorology* (2005) 114: 315–365.
- [25]. Muppa, S.K., Anandan, V.K., Kesarkar, K.A., Rao, S.V.V., Reddy, P.N. Study on deep inland penetration of sea breeze over complex terrain in the tropics. *Atmospheric Research* 104, 209-216, 2012.
- [26]. Murayama, T., Okamoto, H., Kaneyasu, N., Kamataki, H., Miura, K. Application of LIDAR depolarization measurement in the atmospheric boundary layer: Effects of dust and sea-salt particles. *Journal of Geophysical Research*, v. 104, N° D24, 31781-31792, december 27, 1999.
- [27]. Park, S. K., Cobb, E. C., Wade, K., Mulholland, J., Hu, Y., Russell, A. G. Uncertainty in air quality model evaluation for particulate matter due to spatial variations in pollutant concentrations. *Atmospheric Environment*, v.40S563–S573, 2006.
- [28]. Parra, R., Jimenez, P., Baldasano, J.M. Development of the high spatial resolution EMICAT2000 emission model for air pollutants from the north–eastern Iberian Peninsula (Catalonia, Spain). *Environmental Pollution*, v. 140, p. 200–219, 2006.
- [29]. Portelli, R.V. The Nanticoke Shoreline Diffusion Experiment, June 1978-I. Experimental Design and Program Overview. *Atmospheric Environment*, 16, 413 – 421. 1982.
- [30]. Porter, J. N., Horton, K. A., Mouginiis-Mark, P. J., Lienert, B., Sharma, S. K., Lau, E. Sun Photometer and LIDAR measurements of the plume from the Hawaii Kilauea Volcano Pu`uO`o vent: Aerosol flux and SO2 lifetime. *Geophysical Research Letters*, v. 29, n° 16, 10.1029/2002GL014744, 2002.
- [31]. Salvador, N., Loriato, A. G., Santiago, A., Albuquerque, T.T.A., Reis, N. C., Santos, J. M., Landulfo, E., Moreira, G., Lopes, F., Held, G., Moreira, D. M. Study of the Thermal Internal Boundary Layer in Sea Breeze Conditions Using Different Parameterizations: Application of the WRF Model in the Greater Vitória Region, *Revista Brasileira de Meteorologia*, v. 31, n. 4(suppl.), 593-609, 2016a.
- [32]. Salvador, N., Reis, N.C., Santos, J. M., Albuquerque, T.T.A., Loriato, A.G., Santiago, A., Delbarre, H., Augustin, P., Sokolov, A., Moreira, D.M. Evaluation of Weather Research and Forecasting Model Parameterizations under Sea-Breeze Conditions in a North Sea Coastal Environment, *Journal of Meteorological Research, Res.* 30, 998–1018, 2016b.
- [33]. Simon, H., Baker, K.R., Phillips, S. Compilation and Interpretation of Photochemical model Performance Statistics Published between 2006 and 2012. *Atmospheric Environment*, v61, 124-139, 2012.
- [34]. Talbot, C., Augustin, P., Leroy, C., Willart, V., Delbarre, H., Khomenko, G. 2007. Impact of a sea-breeze on the boundary-layer dynamics and the atmospheric stratification in a coastal area of the North Sea. *Boundary-Layer Meteorology*, v125, 133 – 154, 2007a.
- [35]. Talbot, C., Leroy, C., Augustin, P., Willart, V., Delbarre, H., Fourmentin, M., Khomenko, G. Transport and dispersion of atmospheric sulphur dioxide from an industrial coastal area during a sea-breeze event. *Atmos. Chem. Phys. Discuss.*, 7, 15989–16022, 2007b.
- [36]. Vladutescu, D.V., Wu, Y., Gross, M., Moshary, F., Ahmed, S.A., Blake, R.A., Razani, M. Remote Sensing Instruments Used for Measurement and Model Validation of Optical Parameters of Atmospheric Aerosols. *IEEE Transactions on Instrumentation And Measurement*, Vol. 61, No. 6, June 2012.